Journal of Geophysical Research: Oceans

RESEARCH ARTICLE
10.1029/2017JC013628

# The Unusual Surface Chlorophyll Signatures of Southern Ocean Eddies

H. R. S. Dawson[1,2], P. G. Strutton[1,2], and P. Gaube[3]

[1]Institute for Marine and Antarctic Studies, University of Tasmania, Hobart, Tasmania, Australia, [2]Australian Research Council Centre of Excellence for Climate System Science, University of Tasmania, Hobart, Tasmania, Australia, [3]Applied Physics Laboratory, University of Washington, Seattle, WA, USA

**Key Points:**
- We quantify the seasonal and geographical variabilities in the physical and biological characteristics of Southern Ocean mesoscale eddies
- Atypical chlorophyll anomalies are observed in eddies between the Subtropical Front and the Polar Front during summer and autumn
- Eddy stirring, eddy trapping, and eddy pumping all contribute to physical and biological anomalies, depending on the region and season

**Supporting Information:**
- Supporting Information S1
- Table S1

**Correspondence to:**
H. R. S. Dawson,
hannahrsdawson@gmail.com

**Citation:**
Dawson, H. R. S., Strutton, P. G., & Gaube, P. (2018). The unusual surface chlorophyll signatures of Southern Ocean eddies. *Journal of Geophysical Research: Oceans*, *123*, 6053–6069. https://doi.org/10.1029/2017JC013628

Received 22 NOV 2017
Accepted 6 AUG 2018
Accepted article online 13 AUG 2018
Published online 1 SEP 2018



**Abstract** Southern Ocean mesoscale eddies play an important role in ocean circulation and biogeochemical cycling, but their biological characteristics have not been well quantified at the basin scale. To address this, we combined a 15-year tracked eddy data set with satellite observations of ocean color, sea surface temperature, and autonomous profiling floats to quantify the surface and subsurface properties of eddies. Anomalies of surface temperature and chlorophyll were examined in eddy-centric composite averages constructed from thousands of eddies. Normalized surface chlorophyll anomalies ($chl_{norm}$) vary seasonally and geographically. Cyclones typically show positive $chl_{norm}$, while anticyclones have negative $chl_{norm}$. The sign of $chl_{norm}$ reverses during late summer and autumn for eddies between the Subtropical and Polar Fronts. The reversal is most obvious in the Indian sector, and we attribute this to a combination of eddy stirring (deformation of surface gradients by the rotational velocity of an eddy) and deeper winter mixing in anticyclones. Both $chl_{norm}$ and sea surface temperature anomalies transition from dipole structures north of the Subtropical Front to monopole structures south of the Subantarctic Front. Sea surface temperature and $chl_{norm}$ composites provide evidence for eddy trapping (transporting of anomalies) and eddy stirring. This research provides a basin-scale study of surface chlorophyll in Southern Ocean eddies and reveals counterintuitive biogeochemical signals.

**Plain Language Summary** Ocean eddies are spinning parcels of water about 100 km across and 1,500-m deep. They occur everywhere in the ocean. In the Southern Hemisphere, eddies that spin clockwise are cooler than the surrounding ocean because their rotation causes cold, deep water to move upward. This upwelling brings nutrients essential for photosynthesis to the surface and makes clockwise-rotating eddies more productive. Satellites can measure this productivity by sensing differences in ocean color, which result from the increased plankton. By analyzing thousands of Southern Ocean eddies, we found that in summer and autumn, eddies behave opposite to our expectations. That is, clockwise rotating eddies have lower plankton concentrations compared to neighboring waters and counterclockwise rotating eddies have higher concentrations. To explain this, we examined how deep these eddies mix the ocean in the preceding months. We found that counterclockwise rotating eddies mix the ocean deeper in winter, allowing more nutrients to enter their interiors, leading to higher productivity. This work is important because eddy productivity plays a significant role in the exchange of carbon between the ocean and the atmosphere. Carbon exchange in the Southern Ocean is thought to be changing, and this work helps explain an important piece of that process.

## 1. Introduction

The Southern Ocean, defined here as south of 30°S, is an important region for ocean circulation, primary production, and carbon cycling (Frölicher et al., 2015; Landschützer et al., 2015; Sabine et al., 2004). It represents 30% of the global ocean surface area but is responsible for 43% of oceanic anthropogenic carbon dioxide uptake (Frölicher et al., 2015), highlighting its importance in the global climate. The strength of this important carbon sink is variable and sensitive to changes in climate (Landschützer et al., 2015; Le Quéré et al., 2007). Oceanic mesoscale eddies are an essential part of Southern Ocean dynamics (Frenger et al., 2015; Hausmann et al., 2017; Meredith & Hogg, 2006). They create downward fluxes of momentum and energy that transfer into the deep ocean (Holland, 1978) as well as providing important cross-frontal transport of tracers (Dufour et al., 2015; Moreau et al., 2017). Simulations have shown that eddies will offset, at least partially, the increases in Antarctic Circumpolar Current (ACC) transports, which are predicted as a result of the increasingly strong Southern Hemisphere (SH) westerlies (Meredith & Hogg, 2006).

**Table 1**
*A Summary of Chlorophyll and $CO_2$ Signals Observed in Previous Southern Ocean Eddy Studies*

| Region | Cyclones | Anticyclones |
|---|---|---|
| Weddell-Scotia (Kahru et al., 2007) | High chlorophyll | Low chlorophyll |
| NW Georgia Rise (Meredith et al., 2003) | | High chlorophyll |
| Brazil-Malvinas (Gaube et al., 2014) | High chlorophyll monopole | Low chlorophyll monopole |
| Drake Passage | High chlorophyll (Gomez-Enri et al., 2007), reduced iron and community productivity, weak summer $CO_2$ uptake, and winter $CO_2$ sink (Song et al., 2016) | Enhanced iron and community productivity, summer $CO_2$ sink, and winter $CO_2$ source (Song et al., 2016) |

Mesoscale eddies transport heat, salt, energy, nutrients, and phytoplankton throughout the oceans (Chaigneau et al., 2011; Chelton, Schlax, & Samelson, 2011; Dong et al., 2014; Hausmann & Czaja, 2012; McGillicuddy et al., 2007; McGillicuddy & Robinson, 1997). The rotational velocities in eddies can deform horizontal tracer gradients through advection (eddy stirring), and their horizontal propagation can trap and transport tracers from one location to another (eddy trapping; Chelton, Gaube, et al., 2011; Flierl, 1981; McWilliams & Flierl, 1979). Eddies influence biogeochemical cycling by enhancing or suppressing vertical nutrient fluxes and primary production, depending on the vertical velocities at their center (McGillicuddy et al., 2007; McGillicuddy & Robinson, 1997). Cyclones, which rotate clockwise in the SH, typically have higher productivity than their surrounds due to upwelling of nutrient-rich water during their formation and intensification. Conversely, the downwelling of nutrient-depleted surface water during the intensification of anticyclones leads to lower productivity.

Several recent studies have observed productivity anomalies contrary to those predicted due to upwelling and downwelling (Dufois et al., 2014, 2016; Gaube et al., 2013; Waite et al., 2007). For example, anticyclones in the South Indian Ocean (SIO) were shown to have elevated chlorophyll a (hereafter chlorophyll) and enhanced primary production, compared with cyclones, during the SH winter (Dufois et al., 2014; Gaube et al., 2013). Several differing mechanisms have been proposed to explain this high productivity including source water trapping, eddy-induced Ekman pumping, and seasonal modulation of the mixed layer.

Studies of Southern Ocean eddy impacts on biogeochemical cycles and primary production have been difficult because of the poor coverage of satellite data during winter. This has limited the majority of studies to the temperate and tropical oceans, but there are some Southern Ocean examples that serve as background for the work presented here. Kahru et al. (2007) observed elevated chlorophyll biomass in cyclones from the Weddell-Scotia confluence, while anticyclones had lower chlorophyll biomass. In contrast, high chlorophyll concentrations were observed in an anticyclone on the northwest Georgia Rise (Meredith et al., 2003). In the Brazil-Malvinas confluence, cyclones and anticyclones have positive and negative monopoles of normalized chlorophyll anomalies, respectively (Gaube et al., 2014). These monopoles are consistent with trapping of chlorophyll during eddy formation and the vertical flux of nutrients and chlorophyll during eddy intensification (Gaube et al., 2014). Enhanced chlorophyll was observed in cyclones from the Drake Passage (Gomez-Enri et al., 2007). In this same region, cyclones were found to take up less $CO_2$ during the austral summer, whereas anticyclones took up more $CO_2$ (Song et al., 2016). This relationship was reversed in winter. The conclusion to be drawn from these studies, summarized in Table 1 and further explored in this work, is that mesoscale eddies can impact surface chlorophyll and $CO_2$ fluxes in different ways depending on the season and geographical region.

The role of Southern Ocean mesoscale eddies in biogeochemical cycling and productivity is still unclear. Frenger et al. (2015) analyzed their physical properties at a regional to circumpolar scale, and to our knowledge, the only other work to examine their basin-wide impact on surface chlorophyll is Frenger et al. (2018). Given the importance of this region in the global climate, any process, which enhances or suppresses primary production and influences $CO_2$ exchange, as eddies do, is of great importance. Observational based studies are necessary to help evaluate and improve the accuracy of mesoscale-resolving climate models. As the length of the satellite ocean color record increases, the data coverage problems related to cloud cover can be overcome by capturing more eddies. This study is therefore timely and provides a circumpolar analysis of the impact of Southern Ocean eddies on surface chlorophyll.

We aim to extend previous Southern Ocean surface tracer studies (Frenger et al., 2015; Hausmann & Czaja, 2012) to examine the influence of mesoscale eddies on surface chlorophyll. To do so, we combine satellite sea surface temperature (SST), chlorophyll, and Argo-derived mixed layer depths (MLDs) with a 15-year tracked eddy data set. We focus on the seasonal, meridional, and zonal variations in surface chlorophyll and SST anomalies and examine the mechanisms driving these responses. The data sources and methods used are described in section 2. Seasonal and geographical variations in eddy properties and surface tracer anomalies are presented in section 3. Analysis of the mechanisms driving the observed surface tracer responses is discussed in section 4, and we conclude in section 5.

## 2. Data and Methods

### 2.1. Eddy Data Set

The third release of the eddy tracking data set developed by and described in Chelton, Schlax, and Samelson (2011) was used to identify Southern Ocean eddies for 15.5 years from September 1997 to April 2012 (http://cioss.coas.oregonstate.edu/eddies/). This data set includes the latitude and longitude of each eddy observation, the date of observation, the lifetime of the eddy (in weeks), and the amplitude (A), radius (R), rotational velocity (U), and polarity of the eddy. The start date was determined by the beginning of the satellite chlorophyll record, and the end date was the end of the eddy data set. Eddies were identified at seven-day intervals, and each observation of an eddy was referred to as a realization. Thus, if an eddy was observed on 17th September 1997, then this realization is an average of its position during the seven-day period centered on that date. This data set has been used by several authors for regional eddy studies (Dufois et al., 2014, 2016; Gaube et al., 2013, 2014; Hausmann & Czaja, 2012).

### 2.2. Satellite Data

#### 2.2.1. Ocean Color

At high latitudes, the standard algorithms for Sea-viewing Wide Field-of-view Sensor (SeaWiFS) and Moderate Resolution Imaging Spectroradiometer (MODIS) significantly underestimate chlorophyll (Johnson et al., 2013). For this reason, we used eight-day, 9 km SeaWiFS and MODIS ocean color data that were reprocessed using custom Southern Ocean algorithms (Johnson et al., 2013). These data are available from the Integrated Marine Observing System (IMOS) data portal (https://portal.aodn.org.au/search). MODIS and SeaWiFS data were averaged where both existed. The chlorophyll fields were averaged onto a 0.25° grid to be consistent with the resolution of the SSH observations.

The eight-day, 0.25° chlorophyll fields were spatially high-pass filtered using a half-power filter cutoff of 6° in longitude by 6° in latitude. This filtering technique removes oceanographic features with length scales larger than the mesoscale variability of interest (Gaube et al., 2013). The spatially smoothed chlorophyll fields were then subtracted from the original eight-day chlorophyll maps to create high-pass filtered chlorophyll anomalies ($chl_{anom}$). Chlorophyll anomalies were then normalized by dividing the anomaly at a particular longitude ($x$) and latitude ($y$) by the long-term chlorophyll mean at that location (Gaube et al., 2013, 2014);

$$chl_{norm}(x,y) = \frac{chl_{anom}(x,y)}{chl_{ave}(x,y)}$$

The long-term chlorophyll mean was calculated by averaging every eight-day chlorophyll pixel at each latitude and longitude between January 1998 and December 2011. Chlorophyll fields for incomplete years (1997 and 2012) were not used to avoid bias. Normalized chlorophyll anomalies ($chl_{norm}$) created in this fashion retain seasonality and are dimensionless. They can be thought of as a fractional (percentage) departure from the long-term mean. We refer to eddy-averaged chlorophyll concentrations and anomalies in several sections of the paper. These eddy-centric averages were created by computing the mean of all observations within a circle defined by radius R, with center located at the SSH extrema, within each eddy realization.

#### 2.2.2. Sea Surface Temperature

The National Oceanic and Atmospheric Administration (NOAA) 0.25°, daily Advanced Very High Resolution Radiometer (AVHRR)-Only Optimally Interpolated Sea Surface Temperature (OISST) data from September 1997 to April 2012 were used (Reynolds et al., 2007; http://www.ncdc.noaa.gov/oisst/data-access). The OISST product is preferable for this investigation as it interpolates over data gaps. We chose the AVHRR-

only product because it spans the entire altimetric SSH record. The daily OISSTs were averaged to the same seven-day intervals as the eddy observations. These weekly observations were high-pass filtered in the same way as the chlorophyll data, and SST anomalies were constructed by subtracting the weekly high-pass filtered SST fields from the weekly SST climatology. Unlike the chlorophyll fields described above, SST anomalies were not normalized by the long-term mean, because the spatial variations in the background SST field are small when compared to chlorophyll. Normalizing the SST anomalies resulted in anomaly fields with magnitudes that varied significantly with latitude. Thus, comparisons between eddy anomalies from different latitudes were not possible.

### 2.3. Argo Data

We used the MLD climatology developed from Argo profiles by Holte and Talley (2009) to compare mixed layers inside and outside eddies. The MLDs were calculated using a hybrid algorithm, which has the ability to track physical features in the Argo profiles, resulting in more accurate MLD estimates than traditional threshold methods (Holte & Talley, 2009). Argo mixed layer profiles were co-located to eddies by identifying those profiles that surfaced within 0.75R of the eddy center (latitude, longitude), in the same seven-day period as an eddy realization. We chose to average Argo profiles from 0 to 0.75R to capture MLDs within eddy cores. Decreasing the radii resulted in more pronounced mixed layer differences, but greater errors due to the reduced number of data points used to construct the average. Conversely, increasing the radii resulted in less pronounced mixed layer differences. This arises because mixed layer anomalies in eddies decrease with increasing distance from the eddy center (Hausmann et al., 2017).

### 2.4. Average Eddy Composites

We created monthly and seasonal composite averages of satellite and Argo properties to quantify the surface and subsurface structure of eddies. The positions of co-located observations were normalized by R. A value of $\pm 1$ corresponds to the edge of an eddy while 0 corresponds to the eddy core. This allowed us to construct composite averages from eddies of varying sizes. We extracted data from $-2$R to 2R to include the interactions between eddies and the surrounding waters. This method of constructing average eddy composites is frequently used in studies of eddy tracer anomalies (see, e.g., Dufois et al., 2014, 2016; Frenger et al., 2015; Gaube et al., 2013, 2014, 2015; Hausmann et al., 2017; Hausmann & Czaja, 2012).

#### 2.4.1. Surface Satellite Composites

We identified eddy realizations in the same seven- and eight-day time periods as the SST and chlorophyll fields, respectively. The co-located SST and chlorophyll observations in each $2R \times 2R$ box were interpolated onto an evenly spaced 50 by 50 grid to create the surface composite images. The composites were not rotated with the background chlorophyll or SST gradient, so that the axes in each figure point north and east. We did not rotate the composites because the large-scale background SST and chlorophyll gradients are oriented north-south across the Southern Ocean. Rotating eddies to the large-scale SST gradient in the Southern Ocean have previously been found to have negligible impact on the results (Frenger et al., 2015).

#### 2.4.2. Sector Boundaries

Eddies were separated into three ocean sectors; the Indian sector between 20°E and 145°E, the Atlantic sector between 70°W and 20°E, and the Pacific sector between 145°E and 70°W. If an eddy passed from one sector to another, we changed the sector attribution of that eddy, but this happened in less than 1% of eddies. Even long-lived eddies that travel hundreds of kilometers zonally remain in the same ocean basin most of the time (Frenger et al., 2015), justifying our sector-by-sector analysis. Eddies could originate north of 30°S and move south, or originate south of 30°S and move north, but only their time spent south of 30°S was analyzed.

#### 2.4.3. Ocean Fronts

We used the position of the Subtropical Front (STF; Orsi et al., 1995), the northern Subantarctic Front (SAF), and the Polar Front (PF; Sallée et al., 2008) available from the Center for Topographic Studies of the Ocean and Hydrosphere (CTOH; http://ctoh.legos.obs-mip.fr/applications/mesoscale/southern-ocean-fronts), averaged over the chlorophyll period (1997 to 2012), as boundaries for examining meridional variations in properties. We chose to use the SAF and PF positions by Sallée et al. (2008) to be consistent with Frenger et al. (2015), who examined meridional variations in the properties and SST of Southern Ocean eddies. As above, eddies could originate south of the PF and propagate north, or move south across the PF boundary, but only their time spent north of the PF was analyzed.

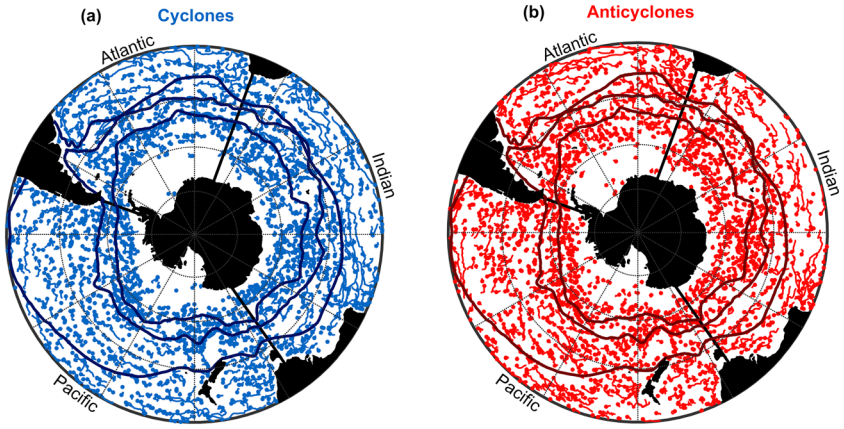


**Figure 1.** Subset of (a) 2000 cyclone tracks and (b) 2000 anticyclone tracks showing the zonal sector divisions and meridional frontal divisions used in this study. Fronts from north to south are the STF, SAF, and PF. The figure shows few eddies crossing between basins and across fronts.

### 2.5. Data Coverage

The coherence of the $chl_{norm}$ composites deteriorates to the south, especially in winter, because ice, cloud cover, and light limitation lead to fewer ocean color observations. For this reason we did not investigate $chl_{norm}$ and SST in eddies south of the PF. We have included the number of eddy realizations in the bottom left corner of all relevant figure panels. During winter between the SAF and the PF we obtained chlorophyll data for 52% of Indian sector eddies, 64% of Atlantic sector eddies, and 15% of Pacific sector eddies. In other seasons between the SAF and the PF we obtained data for between 60% and 98% of eddies. North of the SAF, data were available for 73% to 99% of eddies, depending on the season and region. We used a *t* test to quantify the statistical significance of the composites. Areas that are not statistically significant at the 95% level are indicated by black stippling. To account for correlations between subsequent realizations of the same eddy, we reduced the number of degrees of freedom from the total number of eddy observations in a composite to the number of unique eddy tracks. The area of statistical significance decreases with increasing latitude, especially during winter.

## 3. Results

### 3.1. Eddy Radius, Amplitude, and Velocity

There were 38,660 unique cyclones and 37,758 unique anticyclones observed from September 1997 to April 2012. This corresponds to 485,711 and 474,577 realizations of cyclones and anticyclones, respectively. A map of the study region showing the sector boundaries and a subset of 2,000 cyclone and 2,000 anticyclone tracks is included in Figure 1. Eddy properties are positively skewed toward a greater proportion of eddies with smaller radii, amplitudes, and velocities. The following general statements can be made about eddy properties summarized in Figure S3 and Table S1:

1. There is little difference in the length scale of cyclones and anticyclones. On average, Atlantic sector eddies have the largest radii and Pacific sector eddies have the smallest. As expected, and based on the physical principles governing eddy rotation, radius decreases with increasing latitude.
2. Cyclones have larger amplitudes than anticyclones, consistent with Chelton, Schlax, and Samelson (2011). Zonal differences were observed with Indian sector cyclones having the largest amplitudes (see also Frenger et al., 2015), while Pacific sector eddies of both polarity have the smallest amplitudes. Amplitude also varies with latitude. Eddies between the STF and the SAF generally have the smallest amplitudes, and eddies between the SAF and PF have the largest amplitudes, reiterating the findings of Chelton, Schlax, and Samelson (2011).
3. Rotational velocity scales with amplitude over radius (Chelton, Schlax, & Samelson, 2011). Given the lack of polarity preference for radius and the preference for cyclones to have larger amplitudes, this means that cyclones also have larger velocities than anticyclones. Indian sector cyclones have the fastest velocities and Pacific sector eddies the slowest. Eddies between the SAF and PF have the fastest velocities, whereas those between the STF and SAF have the slowest.

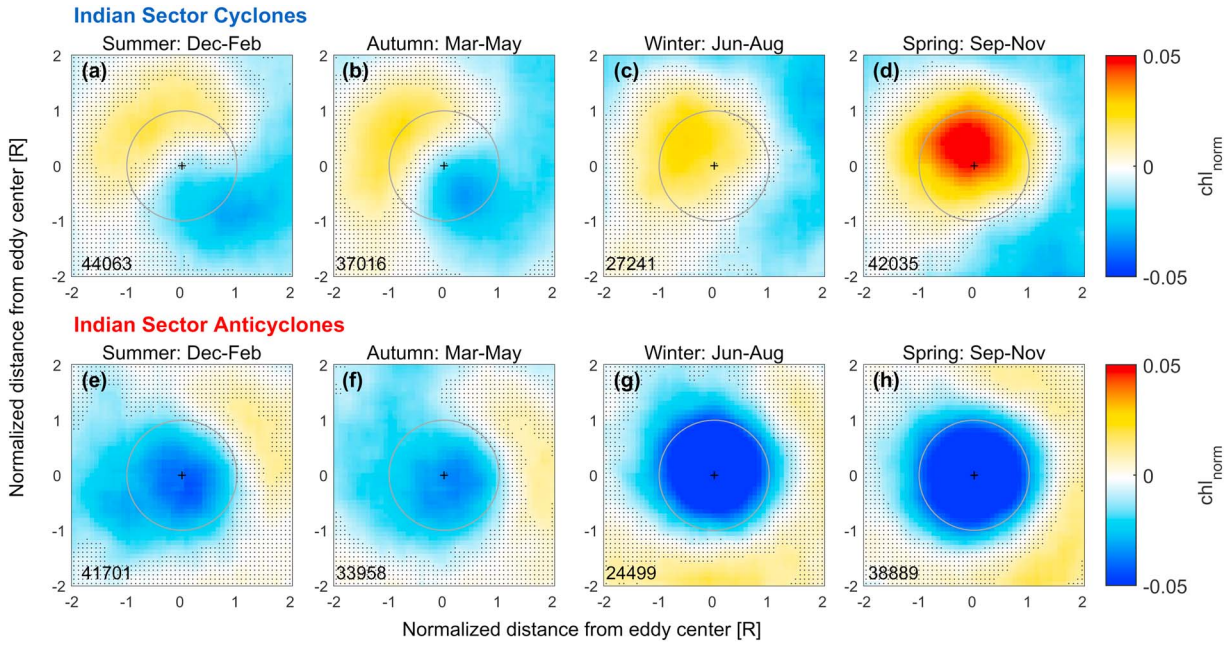


**Figure 2.** Average composites of normalized chlorophyll anomalies ($chl_{norm}$, dimensionless) by season for Indian sector eddies. (a–d) Cyclones in summer, autumn, winter, and spring, respectively. (e–h) Anticyclones in summer, autumn, winter, and spring, respectively. The number of eddy realizations in each composite is shown in the bottom left corner. The grey circle indicates 1R in an idealized eddy with the cross showing the eddy center. The black stippling shows regions where $chl_{norm}$ is not statistically different from zero at the 95% level.

### 3.2. Surface Chlorophyll

#### 3.2.1. Zonal and Seasonal Variabilities in Chlorophyll Anomalies

The biological response to eddies varies seasonally, between basins, and between frontal regions. The seasonal variability of chlorophyll patterns by eddy polarity and basin, but not separated by frontal region, is shown in Figures 2–4. The annual cycle of in-eddy $chl_{norm}$ separated by eddy polarity, basin, and frontal region is shown in Figure 5. After describing these general spatial and temporal patterns, we focus on the Indian sector

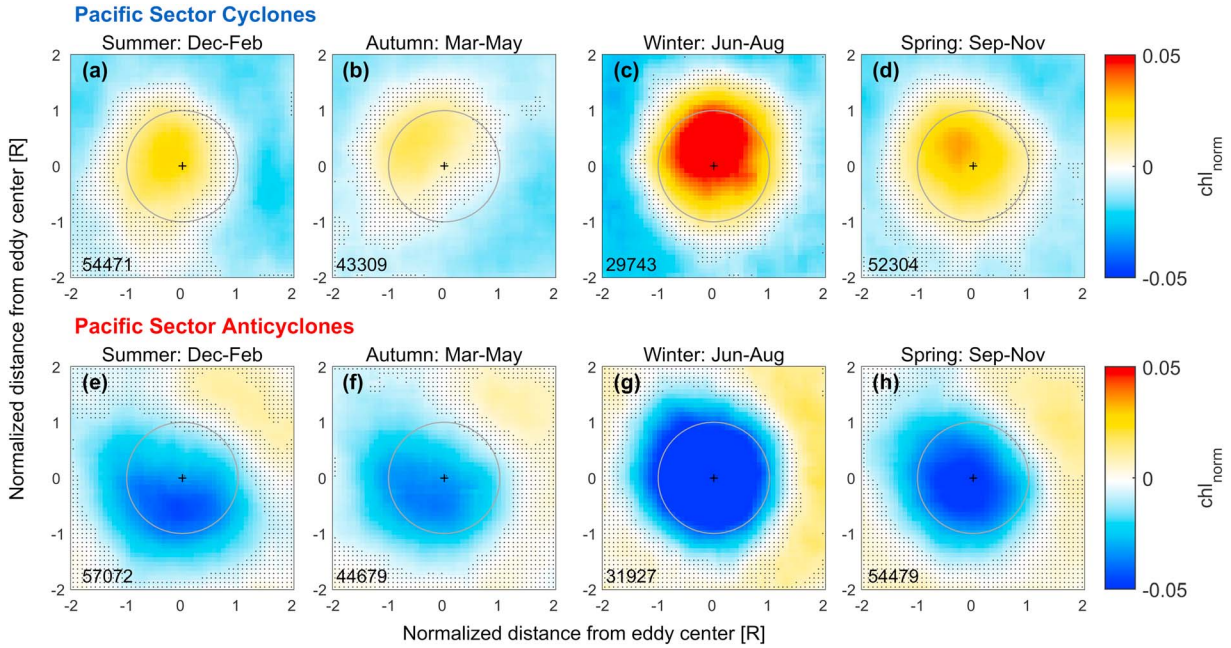


**Figure 3.** Average composites of normalized chlorophyll anomalies ($chl_{norm}$, dimensionless) by season for Pacific sector eddies, otherwise as in Figure 2.

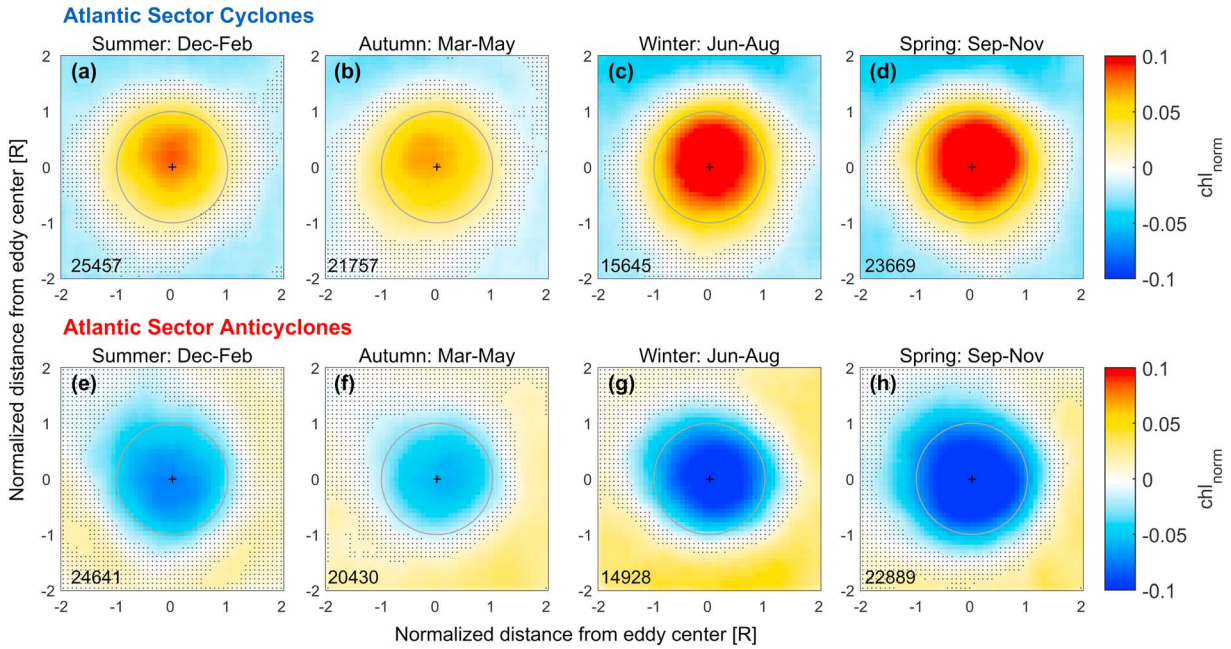


**Figure 4.** Average composites of normalized chlorophyll anomalies ($chl_{norm}$, dimensionless) by season for Atlantic sector eddies, otherwise as in Figure 2. Note that the color scale in Figure 4 is different to Figures 2 and 3.

where some of the more interesting results are most pronounced (Figures 6 and 7). While the figures depict temporal variability at a seasonal resolution, we also inspected monthly plots and will sometimes describe variability at a monthly resolution.

At the basin scale, cyclones have slightly higher chlorophyll concentrations (0.41 ± 0.42 std mg/m$^3$) than anticyclones (0.37 ± 0.38 std mg/m$^3$). Cyclones have positive $chl_{norm}$ (Figures 2a–2d, 3a–3d, 4a–4d, and 5), and anticyclones have negative $chl_{norm}$ (Figures 2e–2h, 3e–3h, 4e–4h, and 5). The sign of these anomalies is as expected based on the rotation and vertical velocities in eddies. For eddies of both polarities, the weakest anomalies, including some months with a reversal in the anomaly sign (sometimes masked by the seasonal averages), occur from January to April (Figure 5). The amplitude of chlorophyll anomalies in eddies peaks in winter to spring for both cyclones and anticyclones in all sectors. The peak occurs slightly earlier in winter for Pacific sector eddies (Figures 3c and 3g), and slightly later in spring for Indian sector eddies (Figures 2d and 2h, 6, and 7).

Chlorophyll concentrations in eddies of both polarity peak in October through December (not shown). Eddies of both polarity in the Atlantic sector have, on average, higher chlorophyll concentrations (more than ±0.55 mg/m$^3$) than eddies in the Indian (less than ±0.38 mg/m$^3$) and Pacific (less than ±0.33 mg/m$^3$) sectors.

### 3.2.2. Meridional and Seasonal Variabilities in Chlorophyll Anomalies

Seasonal trends in the biological response to eddies vary with latitude. South of the STF, $chl_{norm}$ signatures are similar in magnitude between all Southern Ocean sectors. To the north, however, the amplitudes of $chl_{norm}$ are stronger in the Atlantic sector (Figure 5c). Contrary to expectations and to the sector-averaged results described above, anticyclones sometimes have higher chlorophyll than cyclones. Indeed, when separated by frontal zones, seasonal reversals in the sign of $chl_{norm}$ are observed between the STF and the PF (Figure 5d-i). This is the case in the Indian sector between the STF and the SAF from January to May and between the SAF and the PF from March to May (Figures 5d and 5g). It is also true in the Atlantic sector between the SAF and the PF from April to June (Figure 5i).

When examined zonally, the $chl_{norm}$ reversal is most pronounced in the Indian sector, between the STF and the PF (Figures 6e, 6f, and 6j and 7e, 7f, and 7j). Eddies from other ocean basins show a similar reversal in autumn between the SAF and the PF (Figures 5 and S4j to S7j). Interestingly, the reversal is not observed between the STF and the SAF in these other sectors. Pacific sector cyclones have negative $chl_{norm}$ from

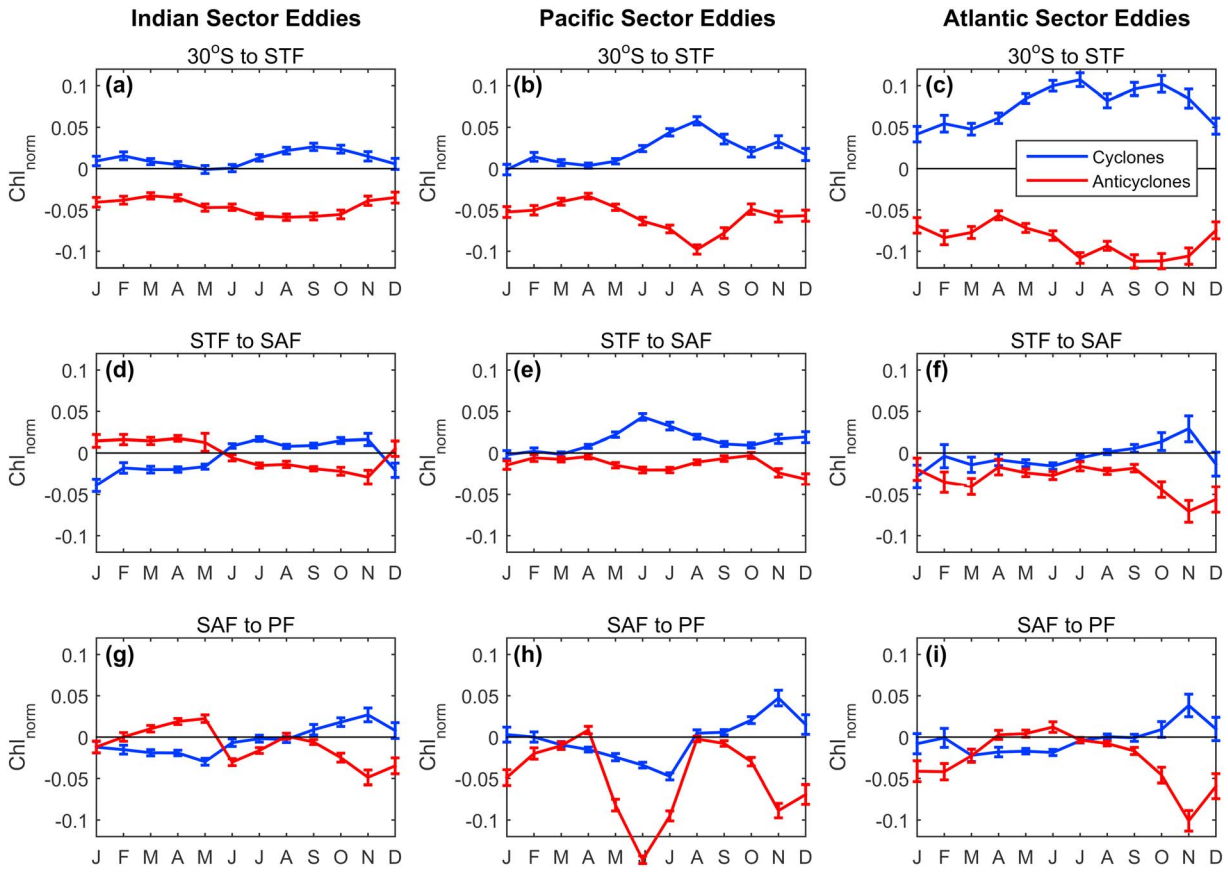


**Figure 5.** Normalized chlorophyll anomalies by month for cyclones (blue) and anticyclones (red) for each frontal region and basin. The first row shows eddies from 30°S to the STF, the second row shows STF to SAF, and the third row shows SAF to PF. (a, d, and g) Indian sector eddies; (b, e, and h) Pacific sector eddies; (c, f, and i) Atlantic sector eddies. The *y* axis extends from −0.13 to 0.13 for (a) to (f) and from −0.16 to 0.16 for (g) to (i). The error bars are standard error (SE) where SE = $s/N_u$, $s$ is the standard deviation, and $N_u$ is the number of unique eddy tracks.

March to July in the region south of the SAF, while Pacific sector anticyclones have weakly positive $chl_{norm}$ in April only (Figure 5h). Atlantic sector cyclones have negative $chl_{norm}$ from March to June south of the SAF (Figure 5 and S6j), and anticyclones have the same pattern of opposite sign (Figures 5 and S7j). The months and locations in which the reversal of $chl_{norm}$ occurred correspond well to the months in which anticyclones have higher chlorophyll (not normalized) than cyclones (data not shown).

### 3.2.3. Variability in the Shape of Chlorophyll Anomalies

The shape of $chl_{norm}$ composites varies both meridionally and zonally. Eddies north of the STF have a spatial structure best described as a dipole of $chl_{norm}$. This dipole pattern is most pronounced in the Indian sector (Figures 6 and 7). In contrast, south of the SAF, $chl_{norm}$ composites are closer to monopoles. In the Indian sector, dipole patterns in cyclones are symmetric in summer and autumn but asymmetric in winter and spring when the zero $chl_{norm}$ line is offset from the eddy center (Figures 6a–6d). The dipole patterns in Indian Ocean cyclones extend from the eddy center up to 2R. Anticyclone dipoles are asymmetric in all seasons, with the larger of the poles centered over the eddy (Figures 7a–7d). These asymmetric dipole patterns are only observed in the surrounding water between 1R and 2R. If we confined out observations to within 1R, the pattern would appear as a monopole.

The most obvious interbasin variations occur between the Atlantic and Indian sectors. Eddies from the Atlantic sector have monopole $chl_{norm}$ structures throughout the year (Figure 4), consistent with previous work from the Brazil-Malvinas confluence (Gaube et al., 2014). In comparison, Indian sector cyclones have dipole $chl_{norm}$ structures within 1R, particularly in the Austral summer and autumn, while Indian sector anticyclones have dipole structures between 1R and 2R. An exception to this is Atlantic sector eddies between the STF and the SAF (Figures S6e– S6h and S7e– S7h), which have strong

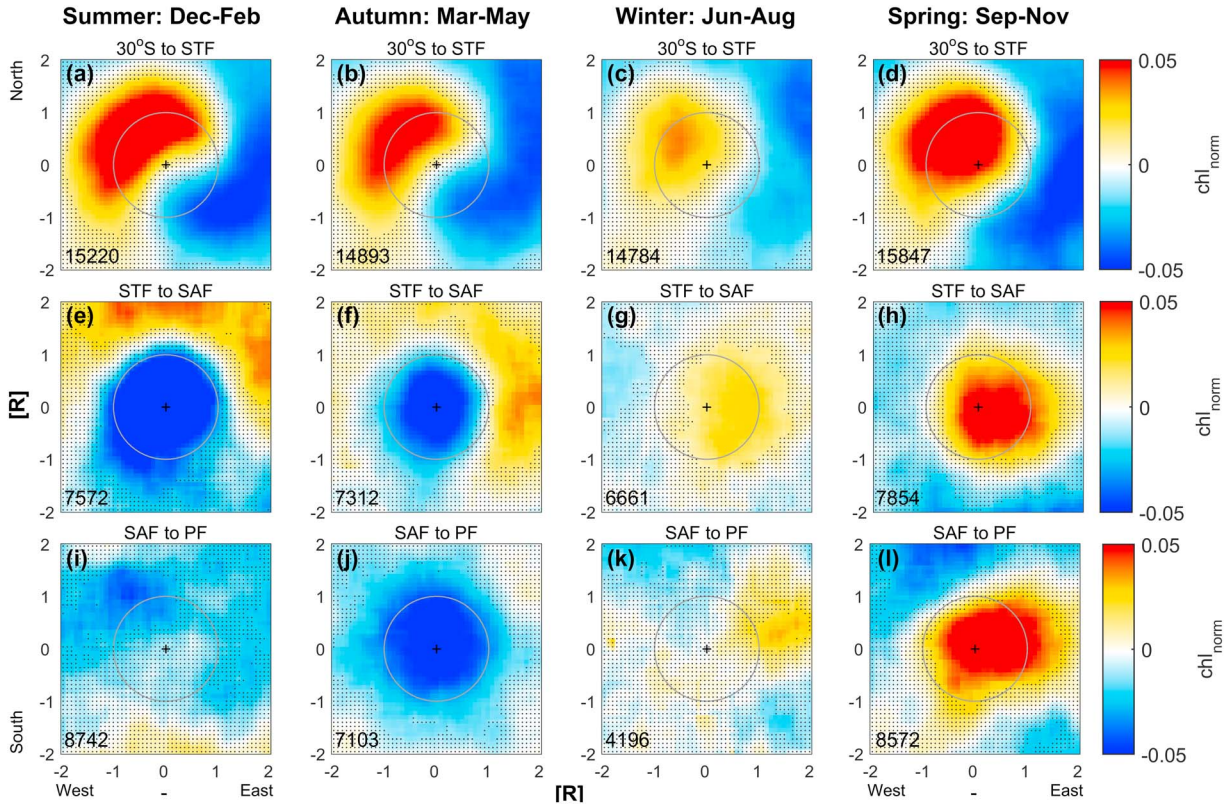


**Figure 6.** Average composites of normalized chlorophyll anomalies ($chl_{norm}$, dimensionless) in Indian sector cyclones by season and frontal region. (a–d) 30°S to STF; (e–h) STF to SAF; (i–l) SAF to PF. The number of eddy realizations used in each composite is shown in the bottom left corner. The grey circle indicates 1R in an idealized eddy with the cross showing the eddy center. The black stippling shows areas where $chl_{norm}$ is not statistically different from zero at the 95% level.

dipole signatures consistent with stirring of a chlorophyll gradient. These dipole signatures extend up to 2R from the eddy center with the maximum anomalies found outside 1R. We return in detail to eddy stirring in the discussion.

#### 3.2.4. Chlorophyll Anomalies in the Indian Ocean Sector

In the Indian sector, the pronounced $chl_{norm}$ reversals in summer and autumn between the STF and SAF have features reminiscent of "tails" extending up to 2R to the south and north for cyclones and anticyclones, respectively (Figures 6e and 6f and 7e and 7f). To explore this further, we examined the background chlorophyll gradient in the Indian sector in greater detail (Figure 8) along with total meridional migration of eddies (not shown). Chlorophyll increases from 30°S to the STF and then decreases from the STF to the PF, excepting summer (Figure 8). Ambient chlorophyll gradients in all frontal regions are stronger in summer and autumn than in winter and spring (Figure 8). On average, cyclones between 30°S and the STF propagate south, but between the STF and the PF they propagate north. Anticyclones between 30°S and the STF propagate north, but between the STF and PF they propagate south. Although this analysis is not shown, the poleward displacement of cyclones and equatorward displacement of anticyclones between 30°S and the STF is evident from the subset of eddy tracks displayed in Figure 1. There is however no statistically significant difference between the seasonal meridional displacement of cyclones and anticyclones in each frontal region.

### 3.3. Sea Surface Temperature

SST anomalies show that the influence of eddies on surface tracers extends outside 1R (Figures 9 and 10). Cyclones have negative SST anomalies compared with their surroundings (−0.21 ± 0.31 °C; Figure 9), and anticyclones have positive SST anomalies (0.25 ± 0.32 °C; Figure 10) in all ocean sectors, consistent with the vertical velocities generated by each type of eddy. That is, cyclones upwell cool, deep water, while anticyclones

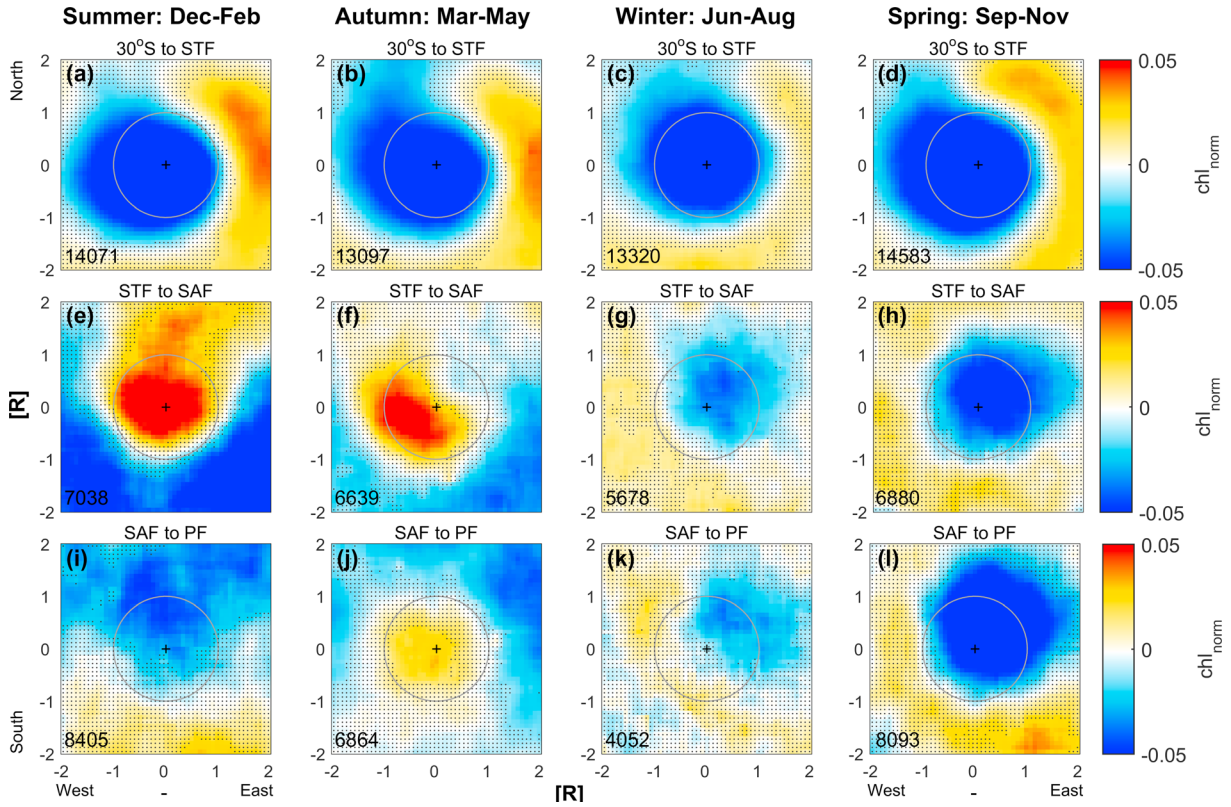


**Figure 7.** Average composites of normalized chlorophyll anomalies ($chl_{norm}$, dimensionless) in Indian sector anticyclones by season and frontal region, otherwise as in Figure 6.

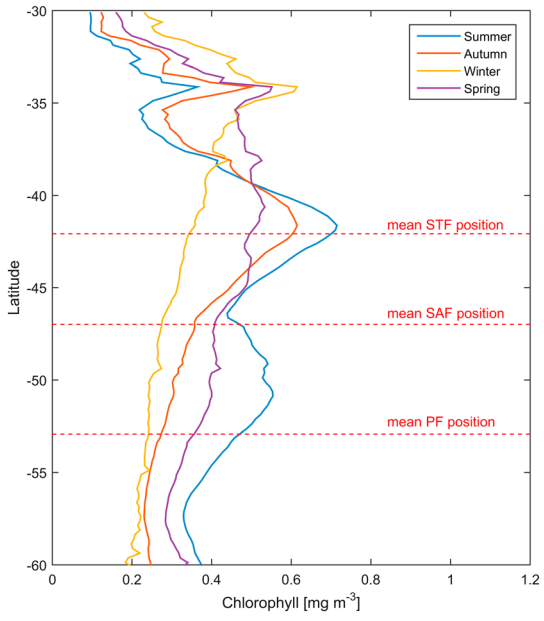


**Figure 8.** Seasonal, background chlorophyll in the Indian sector by latitude. The zonally averaged position of the fronts is shown in red.

downwell warm surface water. The magnitude of SST anomalies is greater in anticyclones than cyclones across all sectors and frontal regions (Table S1).

SST anomalies are weakest in the Pacific sector (less than ±0.20 ± 0.24 °C) and strongest in the Atlantic sector (greater than ±0.27 ± 0.34 °C). The shape and strength of SST anomalies vary meridionally. North of the STF an asymmetric dipole pattern is evident, extending up to 2R from the eddy center (Figures 9a–9d and 10a–10d). Cyclones have cool anomalies over the center and northwest of the eddy and warm anomalies to the east and southeast (Figures 9a–9d). Conversely, anticyclones have warm anomalies over the center and southwest of the eddy and cool anomalies to the east and northeast (Figures 10a–10d). The dipole SST pattern becomes progressively more monopole from summer through to spring, and toward the south, concurrent with an increase in the magnitude of SST anomaly (Frenger et al., 2015; Hausmann & Czaja, 2012). Meridional variations in the shape of SST anomalies are consistent across all ocean basins. For this reason, only composite SST anomalies from eddies across the whole Southern Ocean have been included here (Figures 9 and 10).

### 3.4. MLD Signatures in Eddies

The monthly MLDs in Indian sector cyclones, anticyclones, and eddy-free regions are shown in Figure 11. The Indian sector was chosen because it shows the most significant seasonal reversal in $chl_{norm}$. Deeper winter mixed layers were detected in both SIO anticyclones (Dufois et al., 2014)

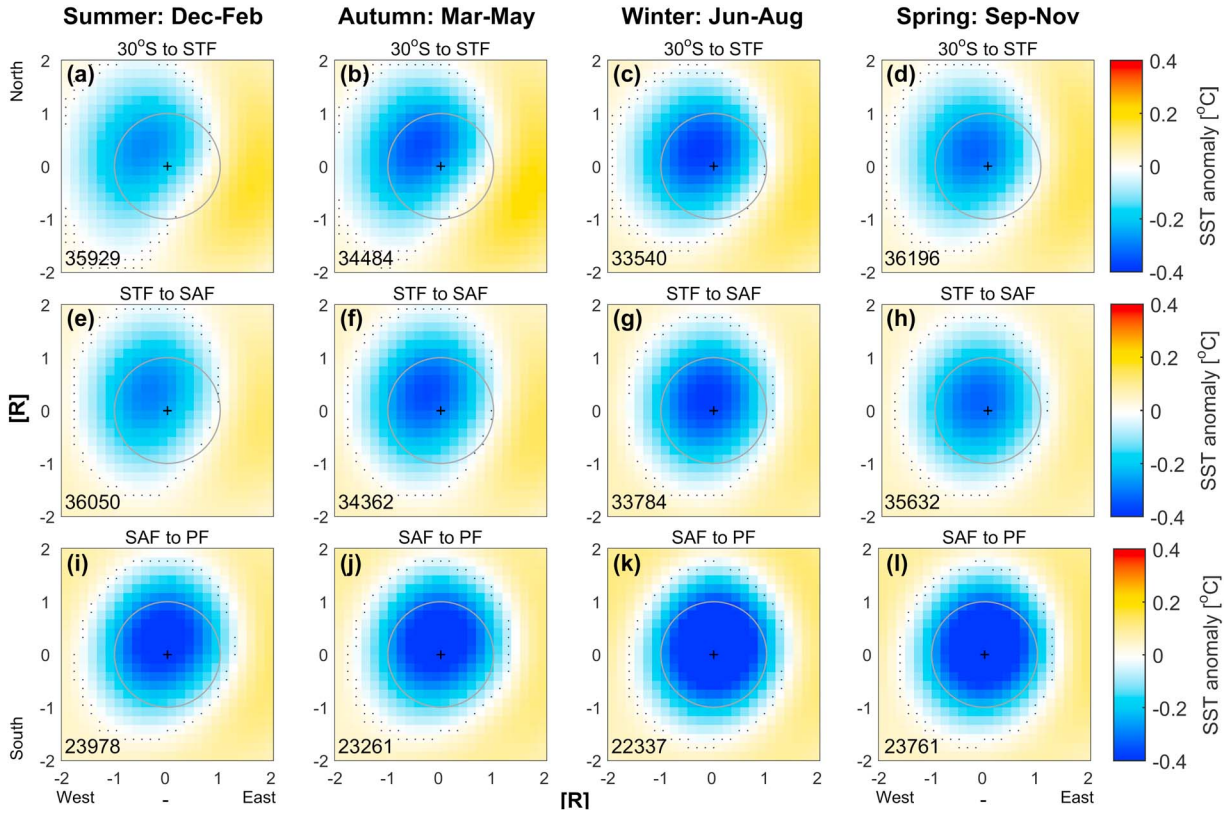


**Figure 9.** Average sea surface temperature anomalies (°C) in cyclones by season and frontal region. (a–d) 30°S to STF; (e–h) STF to SAF; (i–l) SAF to PF. The number of eddy realizations in each composite is shown in the bottom left corner. The grey circle indicates 1R in an idealized eddy with the cross showing the eddy center. The black stippling shows where the SST anomaly is not statistically different from zero at the 95% level.

and Southern Ocean anticyclones, particularly those in the energetic ACC region (Hausmann et al., 2017). As expected, we found that anticyclones have deeper MLDs and cyclones have shallower MLDs than the background average for most of the year but particularly in late winter and spring (Figure 11), consistent with Hausmann et al. (2017). In these months, differences of up to 140 m are observed. During summer and autumn, differences in MLD are small. The peak magnitude of the MLD signature occurs in October for Indian sector eddies between the STF and the SAF (see also Hausmann et al., 2017), but slightly earlier in August and September for eddies north and south of the STF and SAF, respectively.

## 4. Discussion

Dividing the Southern Ocean by sector and frontal zones revealed considerable geographical and seasonal variation in the physics and biology of eddies. The most notable results were as follows:

1. The magnitude of surface tracer anomalies varies meridionally and zonally. SST anomalies are larger in eddies between the SAF and the PF, than north of the STF. Normalized chlorophyll anomalies are stronger in Atlantic sector eddies than in Indian and Pacific sector eddies. This is discussed in section 4.1.
2. The shape of $chl_{norm}$ and SST anomalies also varies meridionally, zonally, and seasonally. North of the STF distinct dipole structures are observed. These dipoles are also more prevalent in the austral summer and autumn, than in winter and spring. Between the SAF and the PF, monopoles dominate. See section 4.2.
3. There is a seasonal switch in the sign of $ch_{lnorm}$ in eddies between the STF and the PF with cyclones showing negative $ch_{lnorm}$ in summer and autumn and anticyclones showing positive $ch_{lnorm}$. This effect is most pronounced in the Indian sector. See sections 4.3 through 4.5.

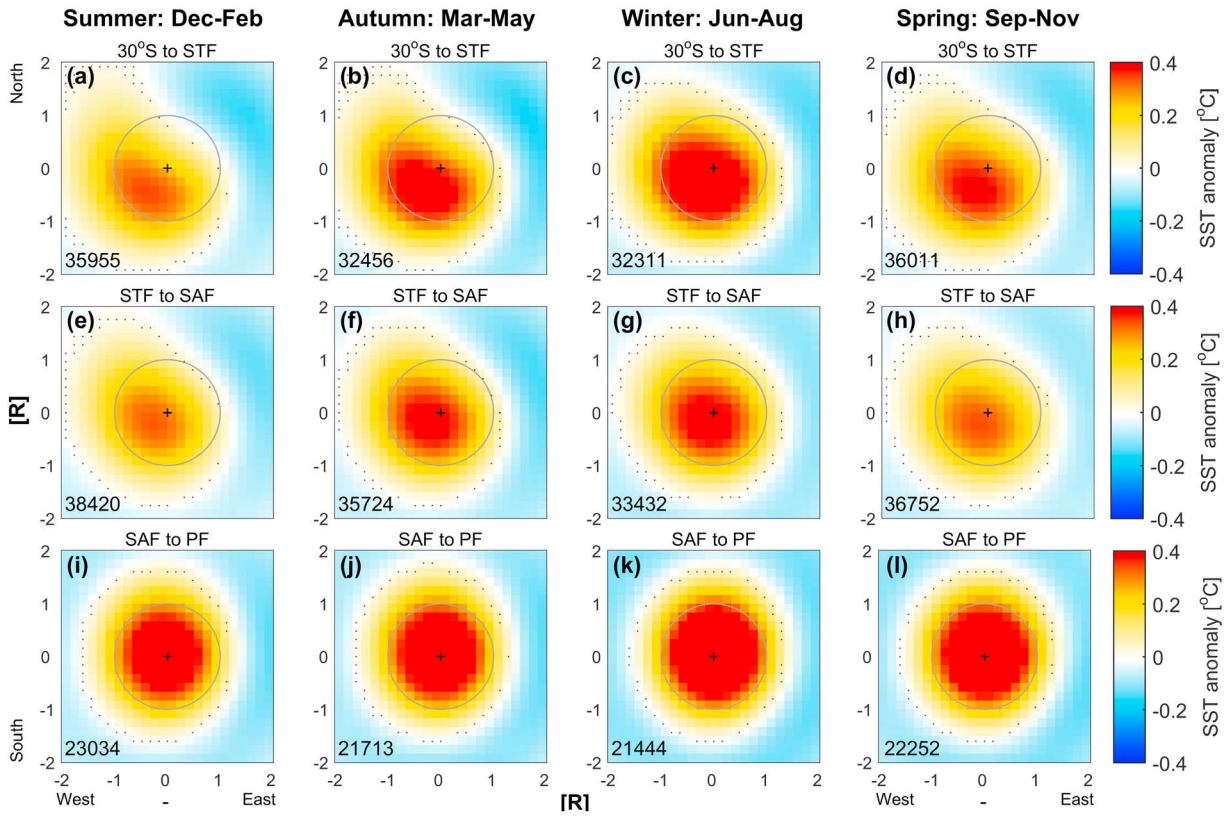


**Figure 10.** Average sea surface temperature anomalies (°C) in Southern Ocean anticyclones by season, otherwise as in Figure 9.

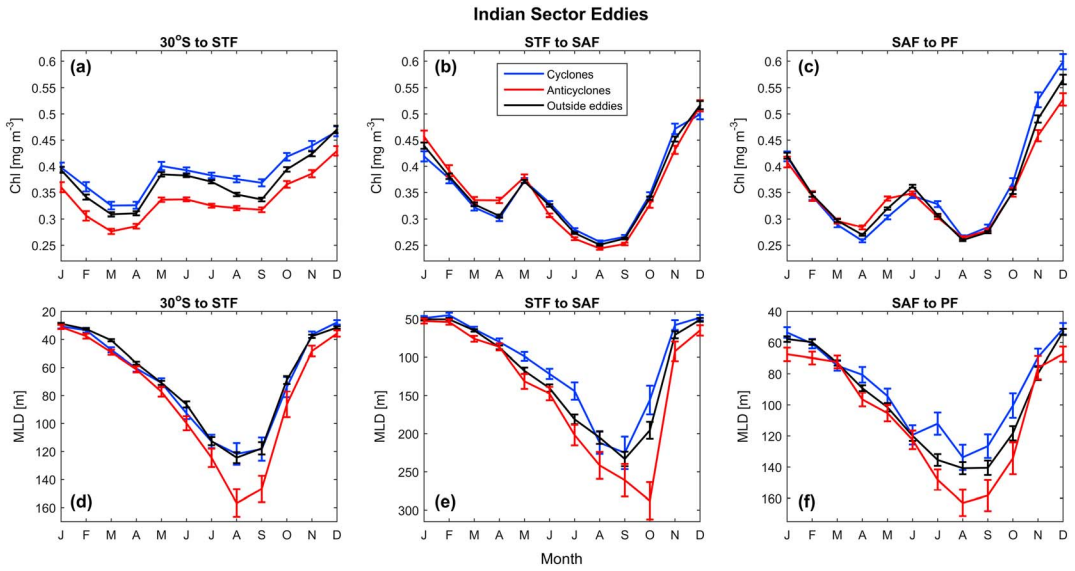


**Figure 11.** (top row) Monthly chlorophyll concentrations and (bottom row) mixed layer depths in Indian sector cyclones (blue), anticyclones (red), and outside eddies (black) from each frontal region. The mixed layer depths inside eddies were averaged from 0 to 0.75R. Note that the *y* axis in the MLD plots varies between frontal regions. The error bars are standard error, where SE = $s/N_u$, $s$ is the standard deviation and $N_u$ is the number of unique eddy tracks.

### 4.1. Variations in Tracer Anomaly Magnitude

In almost all cases, even for monopoles, tracer anomalies extend outside 1R. The radius definition used in this study is based on speed. It identifies a circle with area equal to that enclosed by the SLA contour along which the average geostrophic velocity in the eddy is maximum. Thus, eddy influence on tracer fields is expected beyond the distance R from the eddy center, as is observed in the composite averages presented here.

The magnitude of SST anomalies is greater in anticyclones than cyclones across all basins and frontal regions (Figures 9 and 10 and Table S1). This is perhaps counterintuitive, given that eddies with larger amplitudes and velocities are preferentially cyclonic in the SH (Chelton, Schlax, & Samelson, 2011). Differences in SST magnitude between cyclones and anticyclones were not identified by Frenger et al. (2015) in their Southern Ocean eddy study. We are not able to explain this polarity preference for SST anomalies.

Atlantic sector eddies have stronger $chl_{norm}$ signatures north of the STF (Figure 5c) than eddies from the Indian and Pacific sectors. Average eddy amplitudes and velocities are higher in the Atlantic sector than in the Pacific sector, which might explain the stronger $chl_{norm}$; however, this is not the case when compared with Indian sector eddies (see Table S1). Indeed, Indian sector cyclones were found to have the largest amplitudes and velocities (Table S1; Frenger et al., 2015). As such, we do not invoke differences in eddy amplitude as the reason for stronger $chl_{norm}$ in Atlantic sector eddies. Instead, we attribute this to subsurface nitrate concentrations (WOAv13; Garcia et al., 2013), which are, on average, higher in the Atlantic sector than in the Pacific and Indian sectors. Thus, vertical perturbations in Atlantic sector eddies could bring greater nutrient concentrations into eddies, sustaining higher primary productivity, than perturbations of the same magnitude in Indian and Pacific sector eddies.

### 4.2. Eddy Stirring Versus Trapping

$Chl_{norm}$ composites show similar spatial patterns to surface SST composites. That is, both tracers show dipole structures in the quiescent region north of the STF, but monopole structures in the energetic ACC region south of the STF. These findings are consistent with previous Southern Ocean studies that examined eddy SST composites (Frenger et al., 2015; Hausmann & Czaja, 2012). Hausmann and Czaja (2012) found that eddies from the energetic ACC region had monopole-like SST anomalies, while eddies from quiescent regions in the South Pacific (north of the ACC) showed more dipole-like structures. Similarly, Frenger et al. (2015) found that SST anomalies in ACC eddies were predominantly explained by monopoles, whereas eddies north of the ACC displayed dipoles of SST anomaly.

Eddy surface tracer patterns can be a combination of several processes including eddy stirring (the deformation of background gradients by the rotational velocity of an eddy; Chelton, Gaube, et al., 2011), eddy trapping (advective transport of anomalies; Gaube et al., 2014), eddy pumping (the vertical perturbation of pycnoclines by the formation, growth, and destruction of mesoscale eddies; Huang et al., 2017), and modulation of the mixed layer (convective deepening in anticyclones and restratification and shallowing in cyclones; Hausmann et al., 2017). The dipoles of SST anomaly north of the STF are consistent with eddy stirring of the southward decreasing SST gradient. Cyclones rotating clockwise through this gradient would advect warmer water from the north to the southeast, and cooler water from the south to the northwest, resulting the dipole patterns seen (Figure 9). The reverse patterns are true for anticyclones (Figure 10). Likewise the dipoles of $chl_{norm}$ in the Indian sector north of the STF are consistent with eddy stirring of the southward increasing chlorophyll gradient (Figures 6, 7 and 8). Clockwise rotation of cyclones through this gradient would advect low chlorophyll from the north to the southeast and high chlorophyll from the south to the northwest, as observed in composites from this region (Figure 6). The reverse is true for anticyclones (Figure 7). The asymmetric poles are consistent with perturbation of an ambient gradient by a leading and trailing pole, as discussed in previous literature (Chelton, Gaube, et al., 2011; Frenger et al., 2015; Gaube et al., 2014, 2015; Hausmann & Czaja, 2012).

Moving south across the SAF, both the SST and $chl_{norm}$ anomaly composites transition to monopoles (Figures 6e–6l, 7e–7l, 9e–9l, and 10e–10l), suggesting a process of eddy trapping or eddy pumping during eddy intensification, or both, rather than eddy stirring. A prior study in this region attributed the monopole SST anomalies to eddy trapping (Frenger et al., 2015). The relative contribution from eddy trapping and eddy pumping is hard to ascertain since both give rise to monopoles of the same sign in regions where the cross-current chlorophyll gradient results in trapping of enhanced chlorophyll in cyclones and suppressed chlorophyll in anticyclones (Gaube et al., 2014).

There are several factors that could explain why monopole structures dominate south of the STF. First, the geostrophic current resulting from a given pressure gradient increases as a function of latitude, resulting in faster rotational velocities in eddies of a given amplitude as latitude increases. This is expected to increase the nonlinearity of the eddy and the likelihood of trapping (Chelton, Schlax, & Samelson, 2011; McWilliams & Flierl, 1979). To explore this further, we examined the average nonlinearity of eddies, defined as the ratio of the rotational velocity to the propagation rate, as a function of latitude and season, in each ocean basin (analysis not shown). Indeed, eddies south of the STF in the energetic ACC region have, on average, consistently higher nonlinearity than eddies north of the STF, supporting the eddy trapping hypothesis (Chelton, Schlax, & Samelson, 2011). There are however exceptions to this, in which eddies at certain latitudes north of the STF have higher nonlinearity than those south of the STF. One such example is eddies spawned from the west coast of Australia (Chelton, Schlax, & Samelson, 2011). These peaks of high nonlinearity may be masked in the eddy-centric average composites from this frontal region. Further support for the eddy trapping hypothesis comes from a preliminary investigation into the pattern of $chl_{norm}$ composites over the lifetime of eddies (analysis not shown). This analysis showed that the dominant sign of $chl_{norm}$ was established in the first four weeks, suggesting that eddy trapping is occurring during eddy formation.

A second factor that could explain the monopole structures is that background gradients of chlorophyll and SST are weaker south of the STF (refer to Figure 8 for chlorophyll in the Indian sector). This means that the difference in ambient tracer concentration between the northern and southern edge of an eddy is smaller than north of the STF, leading to less obvious or absent dipole structures.

Dipoles dominate the eddy-centric tracer composites in summer and autumn. We attribute this to stronger background chlorophyll and SST gradients, relative to the eddy diameters, during these seasons. Eddies examined in this study did not show distinct seasonal variations in nonlinearity or physical characteristics at any particular latitude. Thus, there is no evidence to suggest that the dominance of dipoles in these seasons is related to either a lower potential for eddy trapping or variations in eddy characteristics.

### 4.3. Meridional Displacement of Eddies

The Indian sector north of the STF is dominated by long-lived eddies (Frenger et al., 2015). Cyclones in this region, particularly those originating in the eastern Indian sector, have a tendency to propagate poleward. This can be seen in the subset of eddies displayed in Figure 1a, which is consistent with the intrinsic poleward propagation of cyclones (Cushman-Roisin & Beckers, 2011), and is documented in prior literature (Chelton, Schlax, & Samelson, 2011; Frenger et al., 2015). South of the STF, however, the meridional displacement of eddies reverses. We made maps of the total latitudinal displacement of eddies over their lifetime (analysis not shown) and cyclones between the STF and PF propagate equatorward while anticyclones propagate poleward. This is again consistent with both Chelton, Schlax, and Samelson (2011) and Frenger et al. (2015), who identified cyclones moving south to north within the ACC. This average equatorward migration of cyclones and poleward migration of anticyclones between the STF and the SAF is consistent with the tails of $chl_{norm}$ observed from 1R to 2R in composites from this region. It could be interpreted that this lagging tail indicates trapping and subsequent equatorward and poleward displacement of high chlorophyll in cyclones and low chlorophyll in anticyclones, respectively. Yet the lack of statistically significant meridional displacement between seasons fails to explain why these tails are observed in summer and autumn only. However, as discussed at the end of section 4.2, chlorophyll gradients between the STF and the SAF are stronger in summer and autumn than in winter and spring. This means that the same meridional displacement by an eddy could trap and transport strong anomalies during these seasons, leading to the distinct tails observed. What the meridional displacement does not explain is why this tail of $chl_{norm}$ is not observed between the SAF and the PF, despite the meridional displacement of eddies being of the same sign and same order of magnitude as between the STF and the SAF.

Eddy stirring and eddy trapping help to explain much of the variance in surface tracer composites; however, they cannot fully explain the seasonal reversals in $chl_{norm}$ observed between the STF and the PF.

### 4.4. Eddy-Induced Ekman Pumping and Seasonal Chlorophyll Reversals

The summer and autumn $chl_{norm}$ reversals in eddies between the STF and the PF are unusual. Short-lived meanders can sometimes be confused as eddies in satellite altimetry. However, even if we restricted our

analysis to eddies with lifespan greater than 12 weeks, we still observed the seasonal reversal, indicating that meanders are not a dominant factor.

Moreau et al. (2017) also identified low chlorophyll in a cyclonic eddy from the Subantarctic Zone south of Tasmania. The cold-core eddy, which was the subject of a ship-based study from March to April 2016, was found to be less biologically productive than the surrounding water (Moreau et al., 2017). In other regions of the ocean, the SIO, for example, winter reversals have been observed (Dufois et al., 2014, 2016; Gaube et al., 2013). Eddy-induced Ekman pumping has previously been shown to be responsible for anomalously high phytoplankton in anticyclones (Martin & Richards, 2001; McGillicuddy et al., 2007) and has been proposed as a potential driver of anomalous winter chlorophyll reversals (Dufois et al., 2014, 2016; Gaube et al., 2013). Eddy-induced Ekman pumping is created by the superposition of wind-driven Ekman flow on mesoscale eddies. This creates Ekman pumping (downwelling) in cyclones and Ekman suction (upwelling) in anticyclones (Dewar & Flierl, 1987; Flierl & McGillicuddy, 2002; Martin & Richards, 2001; Stern, 1965).

We hypothesized that eddy-driven Ekman pumping may be contributing to generating the unusual reversal in $chl_{norm}$ in eddies from our study region and analyzed total daily Ekman pumping fields ($Wek_{tot}$) from Gaube et al. (2015) in conjunction with chlorophyll composites. The method is described in the supporting information (Text S1 and Figures S1 and S2). There is no distinct seasonal variation in $Wek_{tot}$ that could explain the $chl_{norm}$ reversal in summer and autumn eddies between the STF and the PF. We concluded that the magnitude of eddy-driven Ekman pumping does not change seasonally and we excluded it as a candidate mechanism causing the $chl_{norm}$ reversals.

### 4.5. MLDs and Seasonal Chlorophyll Reversals

Southern Ocean cyclones from the energetic ACC region have shallower winter mixed layers, while Southern Ocean anticyclones have deeper winter mixed layers, compared to their surroundings (Hausmann et al., 2017). Song et al. (2016) suggested that deeper mixing enhanced iron concentrations and community productivity in Drake Passage anticyclones. This effect could similarly increase the concentrations of other nutrients such as nitrate and silicate.

We observed anticyclones with significantly deeper mixed layers and cyclones with significantly shallower mixed layers than the surrounding waters in late winter and spring (Figures 11d–11f). We suggest that deeper winter mixed layers entrain more nutrients, specifically iron, into the interior of anticyclones when compared with the surrounding water and cyclones. Yet the $chl_{norm}$ reversals are not observed until summer and autumn, when there is little difference between the MLD of cyclones and anticyclones. Deeper winter and spring mixed layers, while sourcing deep nutrients, also enhance light limitation, so the biological effect of elevated nutrients in anticyclones might not be seen until later (Song et al., 2016). Nutrients entrained in winter and spring could therefore remain unused in the mixed layer of anticyclones until summer when light limitation is alleviated. At this point they could sustain higher phytoplankton levels inside anticyclones, compared to surrounding water and cyclones, leading to the positive $chl_{norm}$ observed in summer and autumn. Furthermore, as anticyclones have deeper mixed layers, they can continue mixing nutrients into the euphotic zone into spring, whereas the mixing in cyclones is too shallow through most of spring, and thus, phytoplankton communities begin to consume nutrients earlier in the latter. Indeed, low iron concentrations have been observed in a cyclonic eddy during autumn south of Tasmania (Moreau et al., 2017). Vigorous recycling of iron is also likely helping to sustain elevated chlorophyll in anticyclones through summer and autumn (Tagliabue et al., 2016).

We conclude that differential mixing between cyclones and anticyclones, combined with meridional advection of chlorophyll gradients, is the major cause of the seasonal $chl_{norm}$ reversals observed between the STF and the PF.

## 5. Conclusions

We present a basin-scale analysis of surface chlorophyll signatures in Southern Ocean mesoscale eddies. We used surface chlorophyll to investigate spatial and temporal variability, along with SST and Argo-derived MLDs to determine the mechanisms influencing chlorophyll signatures in Southern Ocean eddies. Combining these observations allowed us to (1) investigate differences in eddy tracer advection between sectors and frontal regions, (2) investigate the biological response to eddy circulation, and (3) identify the mechanisms driving this response.

Eddy composites reveal distinct spatial and temporal variations in their physics and biology. Normalized chlorophyll anomalies are stronger in Atlantic sector eddies. We show that this is likely due to stronger vertical nutrient gradients in this basin, rather than variability in eddy characteristics. We suggest that for a given set of eddy characteristics, Atlantic sector eddies can access higher concentrations of deep nutrients and stimulate higher surface productivity more easily than in the Indian and Pacific sectors.

Eddies in the Atlantic sector have predominantly monopole structures of $chl_{norm}$. In contrast, Indian sector cyclones north of the STF have strong symmetric dipoles about the eddy core in summer and autumn, while Pacific sector anticyclones have asymmetric dipoles. Eddy $chl_{norm}$ varies temporally with the weakest anomalies occurring from January to April across most of the Southern Ocean. The strongest anomalies occur in winter for the Pacific sector, spring for the Indian sector, and winter and spring for the Atlantic sector.

Eddy circulation was inferred from the structure of composites. Eddy stirring by the rotational velocity of the eddy is the dominant mechanism influencing tracers north of the STF, particularly in the Indian sector. In contrast, eddy trapping or eddy pumping dominates or acts together between the STF and the PF. We attribute this to (1) faster eddy rotation in this region, which leads to stronger nonlinearity and greater potential for trapping, and (2) the presence of weaker meridional chlorophyll and SST gradients. Eddy stirring dominates the $chl_{norm}$ and SST anomaly composites in summer while eddy trapping or eddy pumping dominates in winter. Again, this is explained by weaker meridional gradients in winter.

We identified unusual high chlorophyll in anticyclones between the STF and the PF in summer and autumn. Positive chlorophyll anomalies have been observed in SIO anticyclones (Dufois et al., 2014, 2016; Gaube et al., 2013). However, these occurred in winter, not summer and autumn as detected here. Atypical chlorophyll reversals are often explained by eddy-induced Ekman pumping, and eddy-driven modulation of the mixed layer. We suggest that deepening of winter and early spring mixed layers in anticyclones and shallowing of mixed layers in cyclones, combined with trapping and meridional advection of background chlorophyll gradients, are the main drivers of the reversals observed here.

Understanding the role of Southern Ocean eddies is critical for parameterization of mesoscale processes in models used to simulate and project ocean biogeochemistry and carbon uptake. However, there are currently few basin-scale biogeochemical data sets available in the Southern Ocean to assist in this understanding. This work provides an observational based study of basin-wide surface chlorophyll in Southern Ocean mesoscale eddies and will help to evaluate and improve the accuracy of mesoscale-resolving climate models. In the future, the large-scale deployment of bio-Argo profiling floats will enable more detailed, basin-scale studies of the subsurface biogeochemical properties in mesoscale eddies.

**Acknowledgments**

The eddy data set used for this study was produced by Dudley Chelton and Michael Schlax (http://wombat.coas.oregonstate.edu/eddies/). The SST data were provided by the National Oceanic and Atmospheric Administration. Wind data used in this study were produced and provided Remote Sensing Systems (http://www.remss.com) and processed by Peter Gaube. The reprocessed Southern Ocean color data were provided by the Integrated Marine Observing System. Argo float data were collected and made freely available by the International Argo Program and the national programs that contribute to it (http://www.argo.ucsd.edu, http://argo.jcommops.org). The Argo Program is part of the Global Ocean Observing System. The mixed layer depth data were provided by the Argo Mixed Layers website (http://mixedlayer.ucsd.edu). The Centre for Topographic studies of the Ocean and Hydrosphere and Australian Antarctic Division provided the Southern Ocean front data used in this study. The data and codes used for this study are available from the author on request. The Australian Research Council Centre of Excellence for Climate System Science provided financial support for this project. Peter Gaube acknowledges funding from NASA grant NNX16AH9G.

## References

Chaigneau, A., Le Texier, M., Eldin, G., Grados, C., & Pizarro, O. (2011). Vertical structure of mesoscale eddies in the eastern South Pacific Ocean: A composite analysis from altimetry and Argo profiling floats. *Journal of Geophysical Research*, *116*, C11025. https://doi.org/10.1029/2011JC007134

Chelton, D. B., Gaube, P., Schlax, M. G., Early, J. J., & Samelson, R. M. (2011). The influence of nonlinear mesoscale eddies on near-surface oceanic chlorophyll. *Science*, *334*(6054), 328–332. https://doi.org/10.1126/science.1208897

Chelton, D. B., Schlax, M. G., & Samelson, R. M. (2011). Global observations of nonlinear mesoscale eddies. *Progress in Oceanography*, *91*(2), 167–216. https://doi.org/10.1016/j.pocean.2011.01.002

Cushman-Roisin, B., & Beckers, J. M. (2011). Fronts, jets and vortices. In *Introduction to geophysical fluid dynamics—Physical and numerical aspects, International geophysics* (Vol. 101, pp. 589–623). Oxford, UK: Elsevier.

Dewar, W. K., & Flierl, G. R. (1987). Some effects of the wind on rings. *Journal of Physical Oceanography*, *17*(10), 1653–1667. https://doi.org/10.1175/1520-0485(1987)017<1653:SEOTWO>2.0.CO;2

Dong, C., McWilliams, J. C., Liu, Y., & Chen, D. (2014). Global heat and salt transports by eddy movement. *Nature Communications*, *5*(1), 3294. https://doi.org/10.1038/ncomms4294

Dufois, F., Hardman-Mountford, N. J., Greenwood, J., Richardson, A. J., Feng, M., Herbette, S., & Matear, R. (2014). Impact of eddies on surface chlorophyll in the South Indian Ocean. *Journal of Geophysical Research: Oceans*, *119*, 8410–8421. https://doi.org/10.1002/2014JC010261

Dufois, F., Hardman-Mountford, N. J., Greenwood, J., Richardson, A. J., Feng, M., & Matear, R. J. (2016). Anticyclonic eddies are more productive than cyclonic eddies in subtropical gyres because of winter mixing. *Science Advances*, *2*(5), e1600282–e1600287. https://doi.org/10.1126/sciadv.1600282

Dufour, C. O., Griffies, S. M., de Souza, G. F., Frenger, I., Morrison, A. K., Palter, J. B., et al. (2015). Role of mesoscale eddies in cross-frontal transport of heat and biogeochemical tracers in the Southern Ocean. *Journal of Physical Ocneaography*, *45*(12), 3057–3081. https://doi.org/10.1175/JPO-D-14-0240.1

Flierl, G., & McGillicuddy, D. J. (2002). Mesoscale and submesoscale physical-biological interactions. In A. R. Robinson, J. J. McCarthy, & B. J. Rothschild (Eds.), *The Sea* (Vol. 12, pp. 113–185). New York: Wiley & Sons.

Flierl, G. R. (1981). Particle motions in large-amplitude wave fields. *Geophysical and Astrophysical Fluid Dynamics*, *18*(1-2), 39–74. https://doi.org/10.1080/03091928108208773

Frenger, I., Münnich, M., & Gruber, N. (2018). Imprint of Southern Ocean eddies on chlorophyll. *Biogeosciences Discussions*, 1–26. https://doi.org/10.5194/bg-2018-70

Frenger, I., Munnich, M., Gruber, N., & Knutti, R. (2015). Southern Ocean eddy phenomenology. *Journal of Geophysical Research: Oceans*, *120*, 7413–7449. https://doi.org/10.1002/2015JC011047

Frölicher, T. L., Sarmiento, J. L., Paynter, D. J., Dunne, J. P., Krasting, J. P., & Winton, M. (2015). Dominance of the Southern Ocean in anthropogenic carbon and heat uptake in CMIP5 models. *Journal of Climate*, *28*(2), 862–886. https://doi.org/10.1175/JCLI-D-14-00117.1

Garcia, H. E., Locarnini, R. A., Boyer, T. P., Antonov, J. I., Baranova, O. K., Zweng, M. M., Reagan, J. R., & Johnson, D. R. (2013). World Ocean Atlas 2013, Volume 4: Dissolved inorganic nutrients (phosphate, nitrate, silicate), S. Levitus, Ed., A. Mishonov technical Ed.; NOAA Atlas NESDIS 76, 1–25. [Available at: http://data.nodc.noaa.gov/woa/WOA13/DOC/woa13_vol4.pdf.]

Gaube, P., Chelton, D. B., Samelson, R. M., Schlax, M. G., & O'Neill, L. W. (2015). Satellite observations of mesoscale eddy-induced Ekman pumping. *Journal of Physical Oceanography*, *45*(1), 104–132. https://doi.org/10.1175/JPO-D-14-0032.1

Gaube, P., Chelton, D. B., Strutton, P. G., & Behrenfeld, M. J. (2013). Satellite observations of chlorophyll, phytoplankton biomass, and Ekman pumping in nonlinear mesoscale eddies. *Journal of Geophysical Research: Oceans*, *118*, 6349–6370. https://doi.org/10.1002/2013JC009027

Gaube, P., McGillicuddy, D. J. Jr., Chelton, D. B., Behrenfeld, M. J., & Strutton, P. G. (2014). Regional variations in the influence of mesoscale eddies on near-surface chlorophyll. *Journal of Geophysical Research: Oceans*, *119*, 8195–8220. https://doi.org/10.1002/2014JC010111

Gomez-Enri, J., Navarro, G., Quartly, G. D., & Villares, P. (2007). Characterizing and following eddies in Drake Passage, *2007 IEEE International Geoscience and Remote Sensing Symposium,* Barcelona, 5117–5120. doi:https://doi.org/10.1109/IGARSS.2007.4424013

Hausmann, U., & Czaja, A. (2012). The observed signature of mesoscale eddies in sea surface temperature and the associated heat transport. *Deep Sea Research Part I: Oceanographic Research Papers*, *70*, 60–72. https://doi.org/10.1016/j.dsr.2012.08.005

Hausmann, U., McGillicuddy, D. J. Jr., & Marshall, J. (2017). Observed mesoscale eddy signatures in Southern Ocean surface mixed-layer depth. *Journal of Geophysical Research: Oceans*, *122*, 617–635. https://doi.org/10.1002/2016JC012225

Holland, W. R. (1978). The role of mesoscale eddies in the general circulation of the ocean—Numerical experiments using a wind-driven quasi-geostrophic model. *Journal of Physical Oceanography*, *8*(3), 363–392. https://doi.org/10.1175/1520-0485(1978)008<0363:TROMEI>2.0.CO;2

Holte, J., & Talley, L. (2009). A new algorithm for finding mixed layer depths with applications to Argo data and subantarctic mode water formation. *Journal of Atmospheric and Oceanic Technology*, *26*(9), 1920–1939. https://doi.org/10.1175/2009JTECHO543.1

Huang, J., Xu, F., Zhou, K., Xiu, P., & Lin, Y. (2017). Temporal evolution of near-surface chlorophyll over cyclonic eddy lifecycles in the southeastern Pacific. *Journal of Geophysical Research: Oceans*, *122*, 6165–6179. https://doi.org/10.1002/2017JC012915

Johnson, R., Strutton, P. G., Wright, S. W., McMinn, A., & Meiners, K. M. (2013). Three improved satellite chlorophyll algorithms for the Southern Ocean. *Journal of Geophysical Research: Oceans*, *118*, 3694–3703. https://doi.org/10.1002/jgrc.20270

Kahru, M., Fiedler, P. C., Gille, S. T., Manzano, M., & Mitchell, B. G. (2007). Sea level anomalies control phytoplankton biomass in the Costa Rica Dome area. *Geophysical Research Letters*, *34*, L22601. https://doi.org/10.1029/2007GL031631

Landschützer, P., Gruber, N., Haumann, F. A., Rödenbeck, C., Bakker, D. C. E., van Heuvan, S., et al. (2015). The reinvigoration of the Southern Ocean carbon sink. *Science*, *349*(6253), 1221–1224. https://doi.org/10.1126/science.aab2620

Le Quéré, C., Rödenbeck, C., Buitenhuis, E. T., Conway, T. J., Langenfelds, R., Gomez, A., et al. (2007). Saturation of the Southern Ocean $CO_2$ sink due to recent climate change. *Science*, *316*(5832), 1735–1738. https://doi.org/10.1126/science.1136188

Martin, A. P., & Richards, K. J. (2001). Mechanisms for vertical nutrient transport within a North Atlantic mesoscale eddy. *Deep Sea Research Part II: Topical Studies in Oceanography*, *48*(4–5), 757–773. https://doi.org/10.1016/S0967-0645(00)00096-5

McGillicuddy, D. J. Jr., Anderson, L. A., Bates, N. R., Bibby, T., Buesseler, K. O., Carlson, A. A., et al. (2007). Eddy/wind interactions stimulate extraordinary mid-ocean plankton blooms. *Science*, *316*(5827), 1021–1026. https://doi.org/10.1126/science.1136256

McGillicuddy, D. J. Jr., & Robinson, A. R. (1997). Eddy-induced nutrient supply and new production in the Sargasso Sea. *Deep Sea Research Part I: Oceanographic Research Papers*, *44*(8), 1427–1450. https://doi.org/10.1016/S0967-0637(97)00024-1

McWilliams, J. C., & Flierl, G. R. (1979). On the evolution of isolated non-linear vortices. *Journal of Physical Oceanography*, *9*(6), 1155–1182. https://doi.org/10.1175/1520-0485(1979)009<1155:OTEOIN>2.0.CO;2

Meredith, M. P., & Hogg, A. M. (2006). Circumpolar response of Southern Ocean eddy activity to a change in the southern annular mode. *Geophysical Research Letters*, *33*, L16608. https://doi.org/10.1029/2006GL026499

Meredith, M. P., Watkins, J. L., Murphy, E. J., Cunningham, N. J., Wood, A. G., Korb, R., et al. (2003). An anticyclonic circulation above the Northwest Georgia Rise, Southern Ocean. *Geophysical Research Letters*, *30*(20), 2061. https://doi.org/10.1029/2003GL018039

Moreau, S., Della Penna, A., Llort, J., Patel, R., Langlais, C., Boyd, P. W., et al. (2017). Eddy-induced carbon transport across the Antarctic Circumpolar Current. *Global Biogeochemical Cycles*, *31*, 1368–1386. https://doi.org/10.1002/2017GB005669

Orsi, A. H., Whitworth, T., & Nowlin, W. D. Jr. (1995). On the meridional extent and fronts of the Antarctic Circumpolar Current. *Deep Sea Research Part I: Oceanographic Research Papers*, *42*(5), 641–673. https://doi.org/10.1016/0967-0637(95)00021-W

Reynolds, R. W., Smith, T. M., Liu, C., Chelton, D. B., Casey, K. S., & Schlax, M. G. (2007). Daily high-resolution-blended analyses for sea surface temperature. *Journal of Climate*, *20*(22), 5473–5496. https://doi.org/10.1175/2007JCLI1824.1

Sabine, C. L., Feely, R. A., Gruber, N., Key, R. M., Lee, K., Bullister, J. L., et al. (2004). The oceanic sink for anthropogenic $CO_2$. *Science*, *305*(5682), 367–371. https://doi.org/10.1126/science.1097403

Sallée, J. B., Speer, K., & Morrow, R. (2008). Southern Ocean fronts and their variability to climate modes. *Journal of Climate*, *21*(12), 3020–3039. https://doi.org/10.1175/2007JCLI1702.1

Song, H., Marshall, J., Munro, D. R., Dutkiewicz, S., Sweeney, C., McGillicuddy, D. J. Jr., & Hausmann, U. (2016). Mesoscale modulation of air-sea $CO_2$ flux in Drake Passage. *Journal of Geophysical Research: Oceans*, *121*, 6635–6649. https://doi.org/10.1002/2016JC011714

Stern, M. E. (1965). Interaction of a uniform wind stress with a geostrophic vortex. *Deep Sea Research and Oceanographic Abstracts*, *12*(3), 355–367. https://doi.org/10.1016/0011-7471(65)90007-0

Tagliabue, A., Aumont, O., DeAth, R., Dunne, J. P., Dutkiewicz, S., Galbraith, E., et al. (2016). How well do global ocean biogeochemistry models simulate dissolved iron distributions? *Global Biogeochemical Cycles*, *30*, 149–174. https://doi.org/10.1002/2015GB005289

Waite, A. M., Pesant, S., Griffin, D. A., Thompson, P. A., & Holl, C. (2007). Oceanography, primary production and dissolved inorganic nitrogen uptake in two Leeuwin current eddies. *Deep Sea Research Part II: Topical Studies in Oceanography*, *54*(8–10), 981–1002. https://doi.org/10.1016/j.dsr2.2007.03.001